3D propagation of the shock-induced vibrations through the whole lower-limb during running

D. Chadefaux [a,b,*], N. Gueguen [c], A. Thouze [c], G. Rao [a]

[a] Aix-Marseille Univ, CNRS, ISM, Marseille, France
[b] Université Paris 13 – Institut de Biomécanique Humaine Georges Charpak (EA 4494), Paris, France
[c] Department of Movement Sciences, Décathlon, Villeneuve d'Ascq, France

Keywords:
Shock-induced vibration
Acceleration
Three-dimensional propagation
Lower-limb
Running

A B S T R A C T

Shock-induced vibrations to the feet have been related to the feel of comfort, the biomechanical control of performance, and the risk of fatigue or injury. Up to recently, the complexity of measuring the human biodynamic response to vibration exposure implied to focus most of the research on the axial acceleration at the tibia. Using wireless three-dimensional accelerometers, this paper investigates the propagation of shock-induced vibrations through the whole lower-limb during running in the temporal and the spectral domains. Results indicated that the vibrations were not consistent across the lower-limb, showing various spatial and spectral distributions of energy. The amount of energy was not constantly decreasing from the distal to the proximal extremity of the runner's lower-limb, especially regarding the lateral epicondyle of the femur. Vibrations in the transversal plane of the segments were substantial compared to the longitudinal axis regarding the distal extremity of the tibia, and the lateral epicondyle of the femur. Further, the spectral content was wider at the distal than at the proximal end of the lower-limb. Finally, to get a thorough understanding of the risks incurred by the runners, the need to account for shock-induced vibrations up to 50 Hz has been stressed when investigating three-dimensional vibrations. The overall study raises attention on the substantial importance of the transverse components of the acceleration, and their potential relation to shear fatigue and injury during running.

1. Introduction

Running is an integral component of many sports, where the impact of the feet on the ground generates vibrations propagating through the entire body. Shock-induced vibrations have been recognized as being influential to the feeling of comfort in the feet (Barrass et al., 2006; Stroede et al., 1999), the biomechanical control of the performance (Chadefaux et al., 2017), and to the risk of fatigue and injury (Lafortune et al., 1996). Repetitive impacts during running have been investigated relative to the risk of injuries such as tibial stress fracture, spinal injuries, or joint and cartilage damages (Lafortune et al., 1996; Milner et al., 2006; Zadpoor and Nikooyan, 2011).

Accelerometers have been used to investigate how vibration is transmitted to the tibia during various running conditions. Using a bone-mounted accelerometer, Lafortune et al. (1991) found that the amount of acceleration reaching the tibia is greater when the running speed increases or when running barefoot. Although the use of bone-mounted accelerometers ensure a better signal quality and a more accurate placement of the sensor than accelerometers fixed to the skin, it requires invasive surgery and prevents investigation of a large number of participants. Therefore, most studies used accelerometers fixed to the skin to facilitate the experimental procedure. Although resulting data differed because of the additional skin and soft tissue artefacts, the observed phenomenon remained coherent (see for instance Lafortune et al. (1991) and Verbitsky et al. (1998)). However, up to recently, most of the investigations of repetitive impacts during running have been limited because of the accelerometer's sensor technology. Indeed, studying the shocks during running requires the use of embedded 3D-accelerometers of high sampling frequency (at least in the range 300–600 Hz, Sheerin et al., 2019), low weight (Valiant, 1990) and dynamics (at least 20 g, Sheerin et al., 2019). Recent progress in this field allowed the use of accelerometers fixed to the skin, to address the axial acceleration of the tibia with respect to various running conditions (Sheerin et al., 2019).

To get a more complete characterization of the shock-induced vibration at the tibia, the three-dimensional components of the

* Corresponding author at: Université Paris 13, UFR SMBH – STAPS, 74, rue Marcel Cachin, 93017 Bobigny, France.
E-mail address: delphine.chadefaux@univ-paris13.fr (D. Chadefaux).

tibial accelerations has been analyzed. Using bone-mounted accelerometers, Lafortune et al. (1991) indicated the importance of the transversal components (i.e. orthogonal to the axial acceleration) with respect to the longitudinal axis. Peaks acceleration at approximately 5.0 g were indeed observed along the anteroposterior and mediolateral axes when running at 3.5 m/s while the longitudinal acceleration was estimated at about 3.0 g. However, due to the complexity and lack of ecological context in running investigation based on bone-mounted accelerometers, the study of the three-dimensional components of the tibial acceleration received little attention until recently. Using a three-dimensional accelerometer, Glauberman and Cavanagh (2014) indicated that non rearfoot strikers present a higher antero-posterior acceleration component that rearfoot strikers. However, using accelerometers fixed on the skin prevented accurate alignment of the sensors axes to the axes of the segments, implying a lack of knowledge about the transversal components (i.e. the ones occurring in the plane orthogonal to the longitudinal component). Consequently, Sheerin et al. (2018) chose to approach studying the vibration magnitude, instead of the three independent axes., Likewise, Giandolini et al. (2016) addressed the transverse shock acceleration relative to the axial component. According to Lafortune et al. (1991), Giandolini et al. (2016) indicated that the vibration magnitude along the transverse plane (approximately 9 g) was similar to the vibration magnitude of the axial acceleration (approximately 10 g) while running downhill. These studies illuminate the importance of the transversal components of the acceleration signal.

Although the tibial acceleration has been widely investigated while running, other parts of the human body have mostly been investigated in light of the propagation of the shock-induced vibrations. In this perspective, papers analyzed the acceleration at the knee (Voloshin and Wosk, 1982), sacrum (e.g. Giandolini et al., 2016), or at the head (e.g. Clansey et al., 2012; Gruber et al., 2014; Valiant, 1990). Studies showed that the acceleration is attenuated from the tibia to the upper-parts of the body and hypothesized on the attenuation processes developed by the musculoskeletal system. This result is also corroborated from a spectral point of view, as several studies stated that the human body acts as a low-pass filter for the input vibration regarding the lower-limb (Edwards et al., 2012, Shorten and Willow, 1992) as well as the upper-limb (Chadefaux et al., 2017).

Research has yet to assess how the shock-induced vibrations propagate throughout the runner's lower-limb along its longitudinal axis and the transverse plane, both in the temporal an spectral domains. Therefore, this paper presents a thorough three-dimensional description of the propagation of the shock-induced vibrations throughout the lower-limb during running. We hypothesize that the lower-limbs' segments act as a low-pass filter regarding both, the longitudinal axis and the transverse plane, and therefore that the amount of vibration is generally, yet irregularly, decreasing from the distal to the proximal extremity of the lower-limb with a complex 3D repartition of the energy.

2. Methods

The experiment was approved by the local university ethics committee in accordance with the Code of Ethics of the World Medical Association (Declaration of Helsinki), and all the subjects signed a consent form.

2.1. Subjects

Ten male participants without noteworthy pathology were involved in the experiments. All participants were regular runners, habituated to running shod, with a rearfoot footfall pattern, and practiced in average 2.5 h per week. Participants were 21 ± 3 years old, 1.80 ± 0.05 m tall, weighted 75 ± 5 kg, their shoes size was 9, 10, or 11.

2.2. Control of the running pattern

Biomechanical data were collected (see Appendix A) to ensure that the running patterns adopted by the participants matched the patterns usually reported in the literature (Novacheck, 1998; Cappelini et al., 2010). Ground reaction forces were collected to detect gait events delimiting the stance phase and to further extract this specific period from the entire database for analysis.

2.3. Measurement protocol

Participants ran in shoes with a 10 mm drop and standard cushioning. In order to avoid fatigue, the experiment was carried out at 90% of the participants' first ventilator threshold (VT1), conveying to $V_{average}$ = 3.1 ± 0.3 m/s. Note that VT1 was determined during a dedicated session, a few days before the main measurement session in an outdoor stadium based on the Ventilatory Equivalent Method (Gaskill et al., 2001).

The day of the experiment, a seven-minute habituation period to the running shoes and speed was performed on a treadmill with a 1% slope (H/P/Cosmos Saturn 250/100 R, Munich, Germany). Participants were then asked to run along a straight line of 25 m and hit the force platform with their right foot (Fig. 1(b)). The force platform was fixed 15 m from the beginning of the running path. To help the participants run at the desired velocity, marks were placed every 5 m on the ground, and audio signals were produced when the participants should be on the mark. To ensure a natural running pattern and that the participants did not target the force platform, participants were asked to look far ahead while running. An unlimited warm-up period was provided to get familiarized to the experimental context. Participants conducted as many trials as required in order to collect seven successful trials, according to the task realization criterion (running speed and visually unperturbed running pattern).

2.4. Shock-induced vibrations

Four tri-axial accelerometers (Noraxon; Arizona, USA; ±24 g pk, [5–1800] Hz, resolution: 0.01 g, mass = 5.7 g, dimensions:

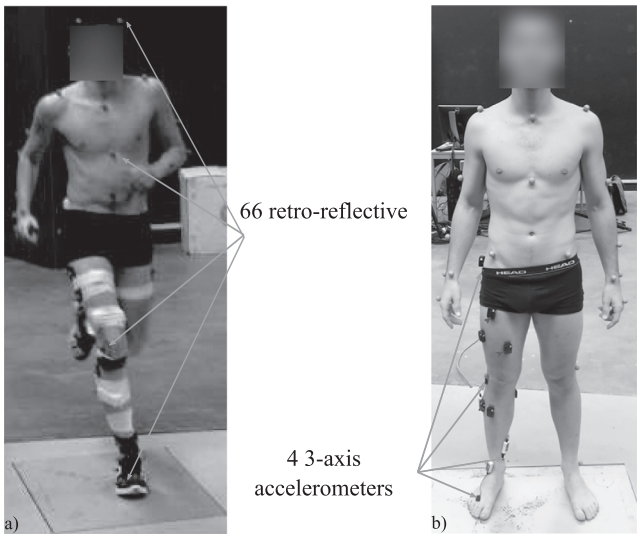

Fig. 1. Participant equipped with four tri-axial accelerometers, and 66 retro-reflective markers before the measurement session (a), and during one trial (b).

1.90 cm × 1.42 cm × 0.63 cm) were placed on the participant's right lower-limb: on the third metatarsal bone (inside the shoe), on the distal extremity of the medial surface of the tibia, on the lateral epicondyle of the femur, and on the greater trochanter of the femur (Fig. 1(a)). Each accelerometer was positioned in such a way as to overlay its x axis with the segment's longitudinal axis. Considering the complexity to align the y and z axes of the accelerometer with the mediolateral and anteroposterior anatomical axes of the investigated segments, the y and z axes were used to describe the transverse components of the acceleration signals. Accelerometers were fixed to the skin using double-sided adhesive tape and secured with adhesive band wrapping the sensors and the body part. The accelerometers were connected to a transmitter by a 9 cm long cable, authorizing the transmitter to be fixed to a non-disturbing position on the lower-limb (Fig. 1(a)). The sampling frequency was 1000 Hz and synchronized with the biomechanical data, and finally segmented over the stance phase. Note that the mass and the size of the accelerometers induced negligible swinging artifacts.

2.5. Descriptors computation

Mean and linear trends were removed from all the collected acceleration signals prior to the descriptors computation. The percent of the stance phase where the maximum of the vibration magnitude was reached (T_{3D}), the amplitude (A_{3D}), and the root-mean-squared (RMS) acceleration level (L_{3D}) of the vibration magnitude were estimated at the third metatarsal bone, the distal extremity of the tibia, the lateral epicondyle of the femur, and the greater trochanter of the femur. The RMS acceleration level of a given vibration was computed according to the definition (IEEE Std 181, 2011)

$$L = \sqrt{\frac{1}{TF_s}\sum_{n=1}^{TF_s}|s_n|^2} \quad (1)$$

for a given discrete signal s_n of duration T and where F_s is the sampling rate. L_{3D} reflects the amount of energy contained in the vibration magnitude at the tibia.

Furthermore, to gain insight into the spatial distribution of the vibration energy conveyed by the shock-induced vibrations at each anatomical point, the ratios $R_x = L_x/L_{3D}$; $R_y = L_y/L_{3D}$; and $R_z = L_z/L_{3D}$ were defined between the RMS acceleration level measured along each axis (L_x, L_y, and L_z) derived from Eq. (1), and the total RMS level L_{3D}.

The ability of the lower-limbs' segments to act as a low-pass filter according to the longitudinal axis, but also the transverse axes was addressed through the spectral content of the shock-induced vibrations. The spectral content of the shock-induced vibrations were analyzed through their power spectra (Tarabini, 2014). The cut-off frequencies F_c of vibration signals propagating through the lower-limb along each axis of the accelerometers were determined from the frequencies for which the spectrum amplitude remains below −3 dB of the maximal passband value. The spectra's shape was described by its spectral centroid

$$\mu = \frac{\sum_{n=1}^{\infty} f_n|P_n(f)|}{\sum_{n=1}^{\infty}|P_n(f)|} \quad (3)$$

where P_n is the power spectrum of the signal s_n and f_n and f are the discrete and the continuous frequency vectors (Peeters, 2004). The 3–8 Hz and the 9–20 Hz bandwidths reflect the *active* (from 30% to 100% of the stance phase, underlining the stabilization of the runner) and *impact* (from 0% to 30% of the stance phase, underlining the shock transmission) phases, respectively (Shorten and Willow, 1992). Consequently, the spectral centroid (μ) has been analyzed on the 3–8 Hz and 9–20 Hz bandwidths (Gruber et al., 2014) to highlight the how the human body manage the shock-induced vibrations with respect to the running phases. As the lower-limb response to vibration is in higher frequencies (Kiiski et al., 2008), the data was also analyzed within the 21–50 Hz bandwidth. These three spectral bandwidths are referred to as low, medium, and high frequency ranges.

2.6. Statistics

In order to describe the three-dimensional propagation of the shock-induced vibrations throughout the runners' lower-limb, each previously defined descriptor (T_{3D}, A_{3D}, L_{3D}, R_x, R_y, R_z, F_c, μ) was investigated regarding both, the observation point and the axis. Repeated analyses of variance analyses were carried out to highlight the effect of the observation point and the axis on the vibrational features. When a significant effect was observed ($p < 0.01$), a multiple comparison of estimated marginal means was carried out to determine the conditions leading to significant differences. Note that only the main effects of the two factors (observation point and direction) were investigated as no physical and physiological meanings in the analysis of the interaction of these two factors have been previously reported.

3. Results

3.1. Vibration analysis in the temporal domain

Fig. 2 and Table 1 summarize the further investigation of how the vibration energy is spatially distributed along the runner's lower-limb. The maximum of the vibration magnitude was reached successively at the third metatarsal bone (T_{3D} = 11.7 ± 4.5% of the stance phase), the distal extremity of the tibia (T_{3D} = 14.6 ± 2.9% of the stance phase), the lateral epicondyle (T_{3D} = 17.0 ± 7.0% of the stance phase) and the greater trochanter of the femur (T_{3D} = 18.4 ± 3.5% of the stance phase). The vibration amplitude was also decreasing from the third metatarsal bone (A_{3D} = 14.5 ± 5.8 g) to the greater trochanter of the femur (A_{3D} = 6.0 ± 2.2 g), but almost no evolution from the distal extremity of the tibia (A_{3D} = 11.5 ± 5.1 g) to the lateral epicondyle of the femur (A_{3D} = 11.0 ± 4.3 g) was reported (Table 1).

The vibration energy at the third metatarsal bone and the greater trochanter of the femur was concentrated along the x-axis (R_x = 47.6 ± 12.2% and R_x = 65.1 ± 9.7, respectively). However, the vibration energy was not as straightforwardly divided between the x-axis (longitudinal to the segment) and the y-z plane (transversal to the segment) regarding the distal extremity of the tibia and the lateral epicondyle of the femur. This spatial distribution of the energy conveyed therefore to a RMS level along the x-axis L_x = 1.9 ± 0.4 g at the third metatarsal bone, L_x = 1.2 ± 0.4 g at the distal extremity of the tibia, L_x = 1.6 ± 0.5 g at the lateral epicondyle of the femur, and L_x = 1.2 ± 0.3 g at the greater trochanter of the femur. In the y-z plane, the RMS level was estimated at $L_{y,z}$ = 2.1 ± 1.1 g at the third metatarsal bone, $L_{y,z}$ = 2.2 ± 1.3 g at the distal extremity of the tibia, $L_{y,z}$ = 2.3 ± 0.6 g at the lateral epicondyle of the femur, and $L_{y,z}$ = 0.6 ± 0.2 g at the greater trochanter of the femur, respectively.

To summarize, the analysis of the vibrations in the temporal domain conveyed that the shock-induced vibrations has a complex three-dimensional repartition along the runner's lower-limb.

3.2. Vibration analysis in the spectral domain

Focusing on the spectral content of the spectral energy along the runner's lower-limb (Fig. 3 and Table 2), the third metatarsal bone and the distal extremity of the tibia presented a wider spectral content than the lateral epicondyle and the greater trochanter

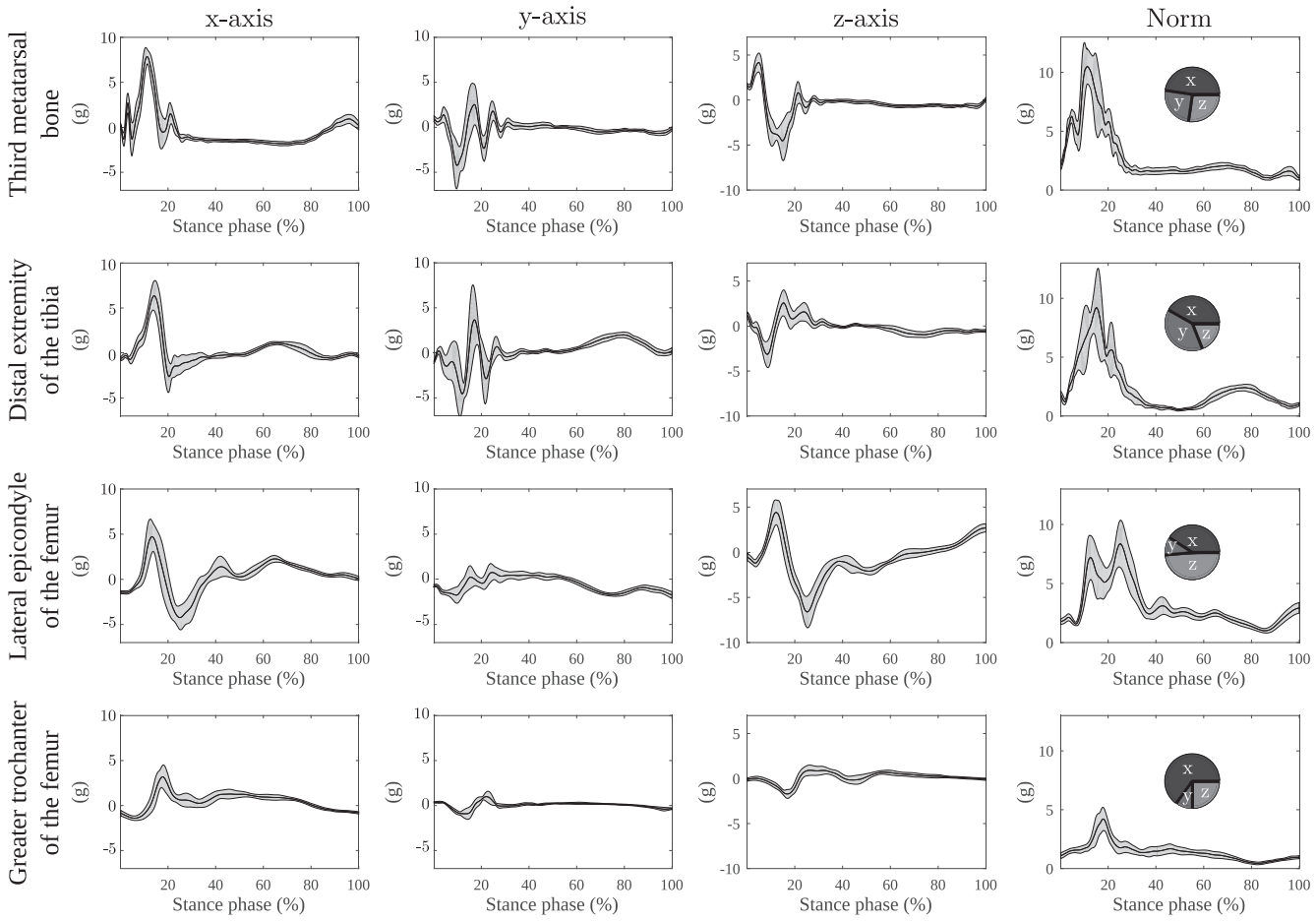

Fig. 2. Vibration signals measured during the stance phase at the third metatarsal bone, the distal extremity of the tibia, the lateral epicondyle and the greater trochanter of the femur along the x, y, and z axes, as well as their vibration magnitude. The black line and the grey area represent the average and the standard deviation estimated over ten participants performing seven repetitions of the task, respectively. Positive values refer to the proximal, the lateral, and the anterior directions. Spatial distribution of the energy estimated along each axis computed over the braking phase are presented associated to each vibration magnitude graph. In the pie charts black, dark grey, and light grey refer to the x, y, and z axes. The averages were computed over ten participants performing seven repetitions of the task.

Table 1
Averaged temporal descriptors computed for each location site on the lower-limb. The averages and standard deviations were computed over ten participants performing seven repetitions of the task. Significant effects ($P < 0.01$) of the location site on the lower-limb on the percent of the stance phase where the maximum of the vibration magnitude was reached (T_{3D}) the amplitude (A_{3D}) and acceleration level (L_{3D}) were pointed out ($F(3, 279) = 84.3$, $F(3,279) = 358.3$, and $F(3,279) = 1123.1$). Finally, a significant effect of the direction on the spatial distribution of the vibration energy (R_x, R_y, R_z) were pointed out ($F(2,209) = 182.5$, $p < 0.01$ for the third metatarsal bone; $F(2,209) = 233.3$, $p < 0.01$ for the distal extremity of the tibia, $F(2,209) = 1641.6$, $p < 0.01$ for the lateral epicondyle, and $F(2,209) = 1080.7$, $p < 0.01$ for the greater trochanter of the femur).

	T_{3D} (%)	A_{3D} (g)	L_{3D} (g)	R_x (–)	R_y (–)	R_z (–)
Third metatarsal bone	11.7 (4.5)	14.5 (5.8)	4.0 (1.2)	47.6 (12.2)	25.1 (11.8)	27.3 (9.0)
Distal extremity of the tibia	14.6 (2.9)	11.5 (5.1)	3.4 (1.3)	41.8 (15.5)	39.2 (18.6)	18.8 (11.2)
Lat. epicondyle of the femur	17.0 (7.0)	11.0 (4.3)	3.9 (0.9)	41.1 (8.9)	10.5 (3.8)	48.1 (10.7)
Greater trochanter of the femur	18.4 (3.5)	6.0 (2.2)	1.8 (0.3)	65.1 (9.7)	10.0 (7.7)	24.9 (8.8)

of the femur along the three axes. The spectral content generated at the third metatarsal bone, the distal extremity of the tibia, and the greater trochanter of the femur contained lower frequencies along the x axis (16.7 ± 11.2 Hz, 27.0 ± 12.1 Hz, and 16.3 ± 7.1 Hz), than along the y axis (41.5 ± 10.6 Hz, 29.9 ± 17.5 Hz, and 29.6 ± 9.5 Hz) and the z axis (27.9 ± 12.1 Hz, 30.6 ± 11.7 Hz, and 19.1 ± 5.4 Hz). On the contrary, the spectral content generated at the lateral epicondyle of the femur contained higher component along the x axis (22.0 ± 3.8 Hz) than the y-axis (10.8 ± 8.5 Hz) and the z-axis (14.8 ± 5.8 Hz).

Considering both the low (LF = [3–8] Hz) and medium (MF = [9–20] Hz) frequency bandwidths defined by (Gruber et al., 2014), as well as the higher frequency content reported in the present study, it seems necessary to introduce an additional high (HF = [21–50] Hz) frequency bandwidth in order to adequately describe the spectral centroid, estimated at 5.6 ± 0.6 Hz, 14.0 ± 1.2 Hz, and 30.9 ± 3.6 Hz. No significant effect of neither the spatial direction nor the location on the runner's lower-limb on the low, medium and high spectral centroids (Table 2) was reported.

4. Discussion

The maximum amplitude of the shock-induced vibration is successively reached from the more distal to the more proximal locations on the lower-limb, and the amount of vibration energy is decreasing from the distal to the proximal extremity of the runner's lower-limb. These results are in accordance with studies

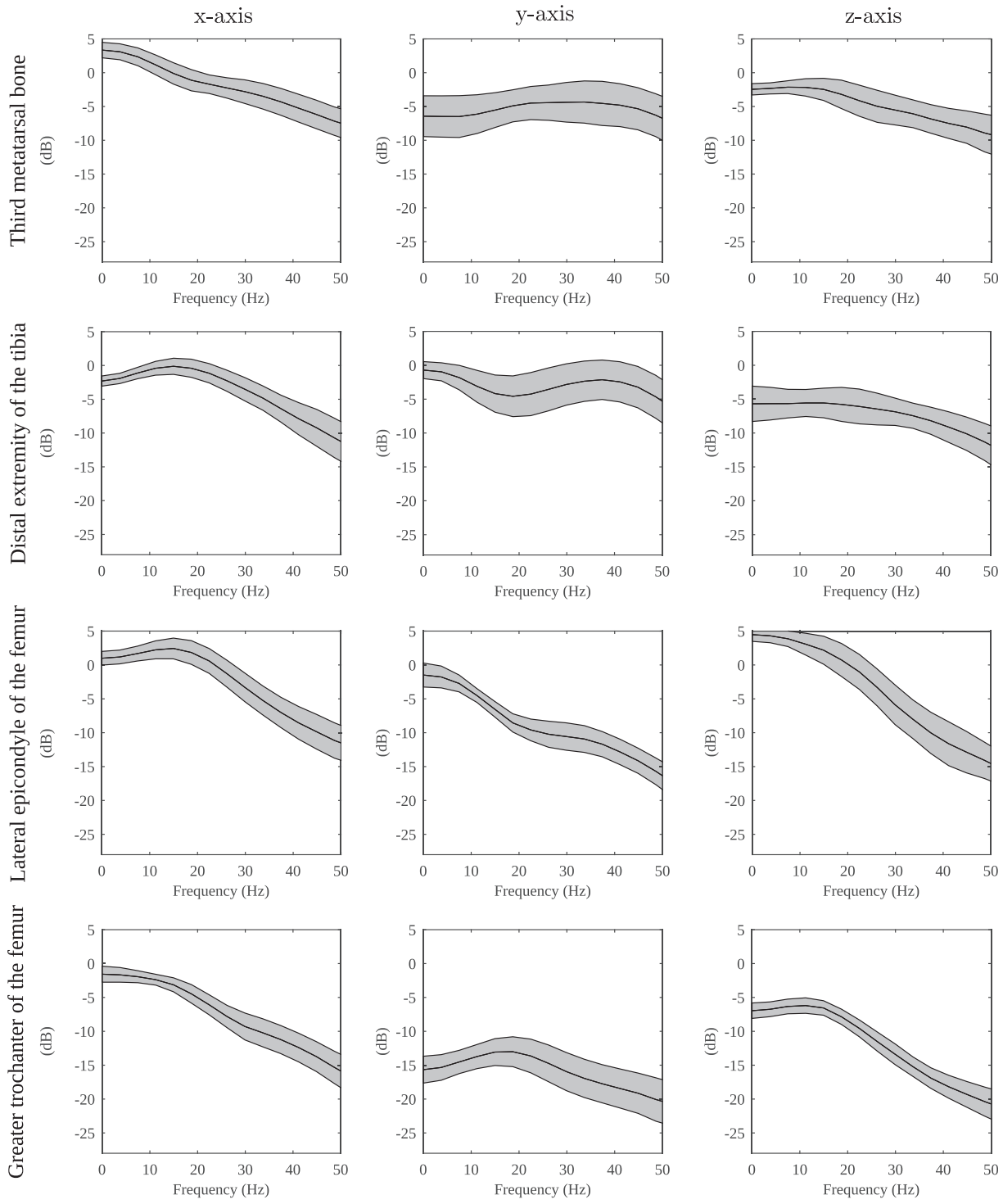

Fig. 3. Spectra of the vibration signals measured at the third metatarsal bone, the distal extremity of the tibia, the lateral epicondyle and the greater trochanter of the femur along the x, y, and z axes. The black line and the grey area represent the average and the standard deviation estimated over ten participants performing seven repetitions of the task. Significant differences in the cut-off frequencies of the vibration signals with the direction ($F(2,209) = 130.6$, $p < 0.01$ for the third metatarsal bone; $F(2,209) = 3.1$, $p = 0.05$ for the distal extremity of the tibia, $F(2,209) = 240.1$, $p < 0.01$ for the lateral epicondyle, and $F(2,209) = 96.1$, $p < 0.01$ for the greater trochanter of the femur), and the location site on the lower-limb ($F(3,279) = 52.4$, $p < 0.01$ for the x-axis; $F(3,279) = 158.4$, $p < 0.01$ for the y-axis; and $F(3,279) = 69.1$, $p < 0.01$ for the z-axis) are highlighted with a dotted line. The reference level is of 10^{-6} m/s^2 (Hagberg et al., 2008).

that have demonstrated the musculoskeletal system's ability to protect its core parts by successively attenuating the shock-induced vibrations (Pratt, 1989). Several processes have been suggested to be involved in cushioning these vibrations: a passive physiological attenuation driven by the mechanical behavior of the anatomical elements (Malekipour et al., 2013); and an active attenuation governed by changes in the orientation of the body segments (Lafortune et al., 1996) or in the activations of the muscular system (Boyer and Nigg, 2007; Wakeling et al., 2003; Khassetarash et al., 2015). Moreover, various shock attenuation mechanisms depending on the frequency bandwidth have been outlined according to the footfall patterns (Gruber et al., 2014).

A detailed examination indicates that the amount of energy reaching the lateral epicondyle of the femur is slightly higher than

Table 2
Averaged spectral descriptors computed for each location site on the lower-limb in low, medium, and high frequencies. The averages and standard deviations were computed over ten participants performing seven repetitions of the task.

		Third metatarsal bone	Distal extremity of the tibia	Lat. epicondyle of the femur	Greater trochanter of the femur
F_c (Hz)	x	16.7 (11.2)	27.0 (6.4)	22.0 (3.8)	16.3 (7.1)
	y	41.5 (10.6)	29.9 (17.5)	10.8 (8.5)	29.6 (9.5)
	z	27.9 (12.1)	30.6 (11.7)	14.8 (5.8)	19.1 (5.4)
μ_{lf} (Hz)	x	5.3 (0.4)	5.9 (0.6)	5.8 (0.6)	5.5 (0.5)
	y	5.6 (0.6)	5.3 (0.5)	5.2 (0.4)	5.8 (0.6)
	z	5.6 (0.5)	5.6 (0.7)	5.5 (0.6)	5.7 (0.6)
μ_{mf} (Hz)	x	13.5 (1.0)	14.4 (0.8)	14.2 (0.8)	13.5 (0.9)
	y	15.1 (1.3)	13.7 (1.3)	12.8 (1.1)	14.7 (1.0)
	z	14.0 (1.1)	14.3 (1.1)	13.4 (1.0)	13.8 (1.0)
μ_{hf} (Hz)	x	31.5 (3.1)	29.5 (2.1)	14.2 (0.8)	29.5 (2.2)
	y	34.3 (2.8)	35.5 (2.8)	12.8 (1.1)	31.1 (3.7)
	z	32.2 (2.9)	31.9 (3.6)	13.4 (1.0)	28.5 (2.4)

at the distal extremity of the tibia. This result suggests that the amount of energy is not constantly decreasing from the distal to the proximal extremity of the runner's lower-limb. This hypothesis is supported by Boyer and Nigg (2007) who showed more evidence of the muscle tuning concept, i.e. of an attenuation process, for the quadriceps than the triceps. Besides, the vibration transmissibility throughout the body has been shown mostly dependent on the knee bending (Tarabini et al., 2013), suggesting that the knee is a key joint in the shock propagation.

In accordance with Giandolini et al. (2016) our results confirmed that more energy was concentrated in the transverse plane than along the longitudinal axis of the third metatarsal bone, the distal extremity of the tibia, and the lateral epicondyle of the femur. On the contrary, the energy was significantly concentrated along the longitudinal axis at the greater trochanter of the femur. Consequently, while the total amount of energy as well as its component along the longitudinal axis were globally decreasing from the third metatarsal bone to the lateral epicondyle of the femur, the amount of energy in the transverse plane remained almost constant up to the lateral epicondyle of the femur and dropped at the greater trochanter of the femur.

The importance of the transverse components during running has also been underlined in Dumas and Jacquelin, 2017. Considering wobbling masses, they showed that the resulting forces at the bone/skin connection were higher along the anteroposterior axis than along the two others at the shank and the thigh, and generally higher at the shank than the thigh. Additionally, the anatomical structures such as the bones are known to be weaker under shear than compression stress (Turner et al., 2001; Bonifasi-Lista et al., 2005). The non-negligible shear stress observed at the distal and proximal extremities of the shank may therefore be related to a risk of fatigue and fatigue failure.

The complex repartition of vibrations observed along the runner's lower-limb may be understood based on the transmissibility of vibrations through the human body. Especially, for a standing subject, it has been shown that an amplification of the vibration occurs between 10 Hz and 25 Hz or 40 Hz for the ankle and the knee (Kiiski et al., 2008), and that the amplified frequency reduces with the knee bending (Yang et al., 2012).

From a spectral point of view, our results indicate that the spectral content is wider at the distal than at the proximal end of the lower-limb. Interestingly, we also highlighted that the spectral content is wider in the transverse plane than along the longitudinal axis at the third metatarsal bone and the greater trochanter of the femur.

At each investigated location on the lower-limb, at least one direction showed a spectral content higher than 20 Hz. Consequently, the usual bandwidths, 3–8 Hz and 9–20 Hz (Gruber et al., 2014) used to study shock-induced vibrations during running should be extended by a third bandwidth up to 50 Hz. Indeed, higher spectral vibrations could imply a higher risk of fatigue and injury for the anatomical element, depending on the frequency their viscoelastic properties (Wu et al., 2012).

A limitation of this study lies in the intrinsic experimental inability to ensure a perfect positioning of surface accelerometers on the runner skin. Although accelerometers were placed on bony-landmarks, soft tissue and skin movement artefacts cannot be entirely avoided.

5. Conclusion

This study has addressed the complex three-dimensional propagation of shock-induced vibrations during running in the temporal and the spectral domains. Interestingly, we observed that the amount of energy is not constantly decreasing from the distal to the proximal extremity of the runner's lower-limb. Our results shed light on the importance of taking account for the three components of the shock-induced vibration with respect to a risk of shear fatigue and injury. The need to account for shock-induced vibrations up to 50 Hz has also been stressed.

Declaration of Competing Interest

None.

Acknowledgements

The authors would like to thank Sébastien Garcia and Bastien Delarieu for their involvement in the measurements; runners who participated in this study, as well as Katie Goggins for proofreading the paper.

Disclosure statement

Authors disclose professional relationships with companies or manufacturers who will benefit from the results of the present study. The results of the study are presented clearly, honestly, and without fabrication, falsification, or inappropriate data manipulation.

Appendix A. Biomechanical analysis

A force platform (Kistler 9287CA; Winterthour, Swiss) was used to measure the ground reaction forces of the participant's right foot impact at 2000 Hz. The resulting vertical component was used to determine the stance phase over the force platform. This period was defined as the instants when the vertical component of the

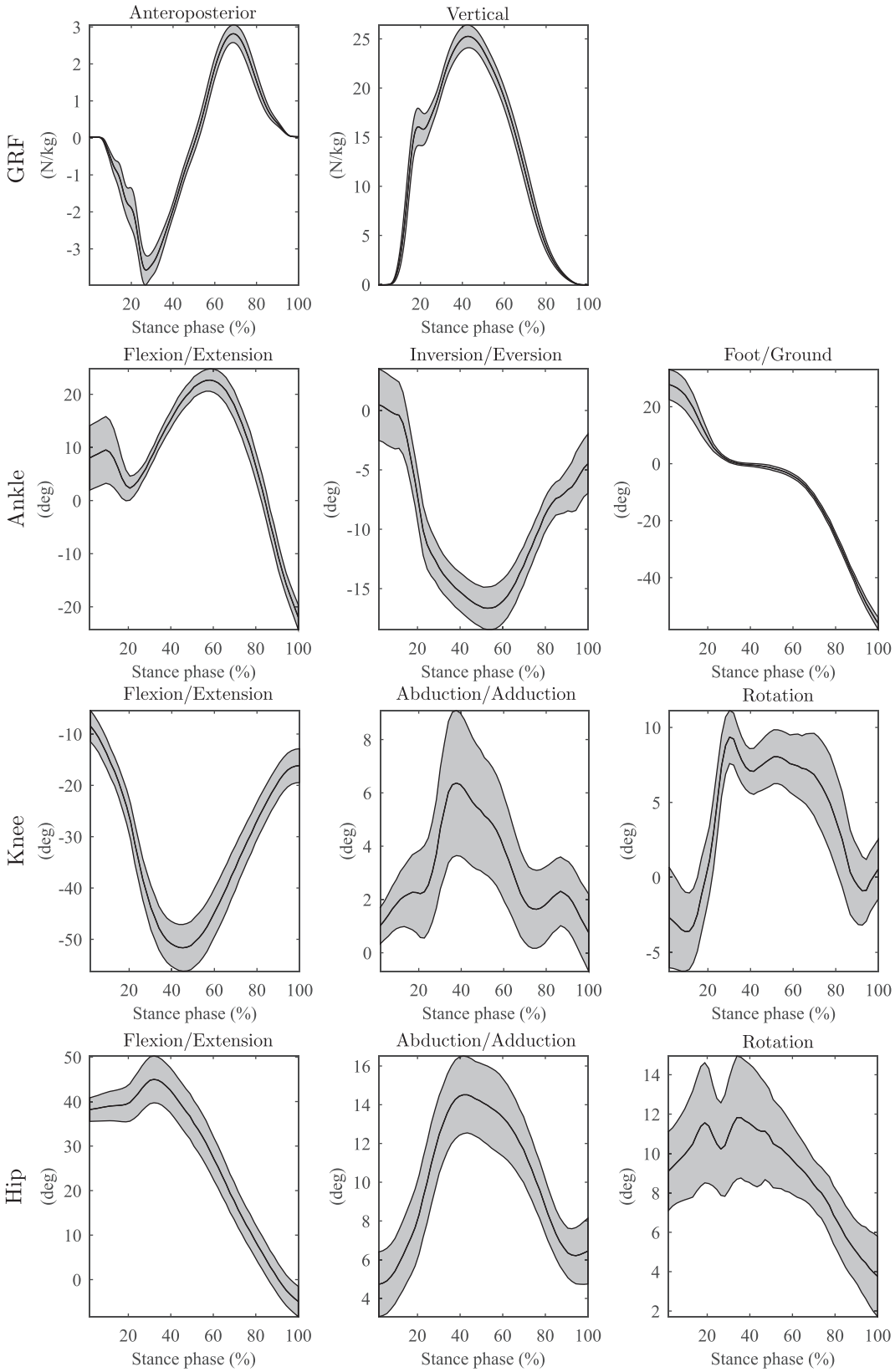

Fig. A1. Averaged ground reaction forces and kinematics of the right lower-limb during the stance phase. The ground reaction forces are adimensionalized by the participant's mass. Positive values refer to the ankle flexion and eversion; the knee extension, adduction and intern rotation; the hip flexion, adduction, and extern rotation. The zero value of each angle is referring to the standard anatomical position. The averages are computed over ten participants performing seven repetitions of the task.

force exceeds 20 N. A high-resolution motion-capture system (Qualisys Oqus, Gothenburg Sweden) was used to capture whole-body kinematics at 200 Hz (Fig. 1(a)). All the kinematics database was segmented from the beginning to the end of the stance phase. The ground reaction forces and kinematics of the right lower-limb during the stance phase were consistent across the participants and matched the profiles from the literature (Novacheck, 1998); see Fig. A1 for more information.

References

Barrass, D.F., Roberts, J.R., Jones, R., 2006. Assessment of the impact sound in golf putting. J. Sports Sci. 24 (5), 443–454.

Bonifasi-Lista, C., Lake, S.P., Small, M.S., Weiss, J.A., 2005. Viscoelastic properties of the human medial collateral ligament under longitudinal, transverse and shear loading. J. Orthopaetic Res. 23 (1), 67–76.

Boyer, K.A., Nigg, B.M., 2007. Changes in muscle activity in response to different impact forces affect soft tissue compartment mechanical properties. J. Biomech. Eng. 129 (4), 594–602.

Cappellini, G., Ivanenko, Y.P., Dominici, N., Poppele, R.E., Lacquaniti, F., 2010. Migration of motor pool activity in the spinal cord reflects body mechanics in human locomotion. J. Neurophysiol. 104 (6), 3064–3073.

Chadefaux, D., Rao, G., Androuet, P., Berton, E., Vigouroux, L., 2017. Active tuning of stroke-induced vibrations by tennis players. J. Sports Sci. 35 (16), 1643–1651.

Clansey, A.C., Hanlon, M., Wallace, E.S., Lake, M.J., 2012. Effects of fatigue on running mechanics associated with tibial stress fracture risk. Med. Sci. Sports Exerc., 1917–1923

Dumas, R., Jacquelin, E., 2017. Stiffness of a wobbling mass models analysed by a smooth orthogonal decomposition of the skin movement relative to the underlying bone. J. Biomech. 62, 47–52.

Edwards, W.B., Derrick, T.R., Hamill, J., 2012. Musculoskeletal attenuation of impact shock in response to knee angle manipulation. J. Appl. Biomech. 28, 502–510.

Giandolini, M., Horvais, N., Rossi, J., Millet, G.Y., Samozino, P., Morin, J.B., 2016. Foot strike pattern differently affects the axial and transverse components of shock acceleration and attenuation in downhill trail running. J. Biomech. 49 (9), 1765–1771.

Gaskill, S.E., Ruby, B.C., Walker, A.J., Sanchez, O.A., Serfass, R.C., Leon, A.S., 2001. Validity and reliability of combining three methods to determine ventilatory threshold. Med. Sci. Sports Exerc. 33 (11), 1841–1848.

Glauberman, M.D., Cavanagh, P.R., 2014. Rearfoot strikers have smaller resultant tibial accelerations at foot contact than non-rearfoot strikers. J. Foot Ankle Res. 7, A93.

Gruber, A.H., Boyer, K.A., Derrick, T.R., Hamill, J., 2014. Impact shock frequency components and attenuation in rearfoot and forefoot running. J. Sport Health Sci. 3 (2), 113–121.

Hagberg, M., Burstrom, L., Lundstrom, R., Nilsson, T., 2008. Incidence of Raynaud's phenomenon in relation to hand-arm vibration exposure among male workers at an engineering plant a cohort study. Journal of Occupational Medicine and Toxicology 3 (13), 1–6.

IEEE Instrumentation and Measurement Society, 2011. IEEE Standard for Transitions, Pulses, and Related Waveforms. Revision of IEEE Std 181-2003.

Khassetarash, A., Hassannejad, R., Enders, H., Ettefagh, M.M., 2015. Damping and energy dissipation in soft tissue vibrations during running. J. Biomech. 48 (2), 204–209.

Kiiski, J., Heinonen, A., Järvinen, T.L., Kannus, P., Sievänen, H., 2008. Transmission of vertical whole body vibration to the human body. J. Bone Miner. Res. 23 (8), 1318–1325.

Lafortune, M.A., 1991. Three-dimensional acceleration of the tibia during walking and running. J. Biomech. 24 (10), 877–996.

Lafortune, M.A., Hennig, E.M., Lake, M.J., 1996. Dominant role of interface over knee angle for cushioning impact loading and regulating initial leg stiffness. J. Biomech. 29 (12), 1523–1529.

Malekipour, F., Whitton, C., Oetomo, D., Lee, P.V., 2013. Shock absorbing ability of articular cartilage and subchondral bone under impact compression. J. Mech. Behav. Biomed. Mater. 26, 127–135.

Milner, C.E., Ferber, R., Pollard, C.D., Hamill, J., Davis, I.S., 2006. Biomechanical factors associated with tibial stress fracture in female runners. Med. Sci. Sports Exerc. 38 (2), 323–328.

Novacheck, T.F., 1998. The biomechanics of running. Gait & Posture 7 (1), 77–95.

Peeters, G., 2004. A Large Set of Audio Features for Sound Description (Similarity and Classification) in the CUIDADO Project. Technical Report; IRCAM, Paris, France.

Pratt, D.J., 1989. Mechanisms of shock attenuation via the lower extremity during running. Clin. Biomech. 4 (1), 51–57.

Sheerin, K.R., Besier, T.F., Reid, D., Hume, P.A., 2018. The one-week and six-month reliability and variability of three-dimensional tibial acceleration in runners. Sports Biomech. 17 (4), 531–540.

Sheerin, K.R., Reid, D., Besier, T.F., 2019. The measurement of tibial acceleration in runners – A review of the factors that can affect tibial acceleration during running and evidence-based guidelines for its use. Gait Posture 67, 12–24.

Shorten, M.R., Willow, D.S., 1992. Spectral analysis of impact shock during running. Int. J. Sport Biomech. 8, 288–304.

Stroede, C.L., Noble, L., Walker, H.S., 1999. The effect of tennis racket string vibration dampers on racket handle vibrations and discomfort following impacts. J. Sports Sci. 17, 379–385.

Tarabini, M., Saggin, B., Scaccabarozzi, D., Gaviraghi, D., Moschioni, G., 2013. Apparent mass distribution at the feet of standing subjects exposed to whole-body vibration. Ergonomics 56 (5), 842–855.

Tarabini, T., Solbiati, S., Moschioni, G., Saggin, B., Scaccabarozzi, D., 2014. Analysis of non-linear response of the human body to vertical whole-body vibration. Ergonomics 57 (11), 1711–1723.

Turner, C.H., Wang, T., Burr, D.B., 2001. Shear strength and fatigue properties of human cortical bone determined from pure shear tests. Calcif. Tissue Int. 69 (6), 373–378.

Valiant, G.A., 1990. Transmission and attenuation of heelstrike accelerations. In: Cavanagh, P.R. (Ed.), Biomechanics of Distance Running. Human Kinetics, Champaign, IL, pp. 225–247.

Verbitsky, O., Mizrahi, J., Voloshin, A., Treiger, J., Isakov, E., 1998. Shock transmission and fatigue in human running. J. Appl. Biomech. 14, 300–311.

Voloshin, A., Wosk, J., 1982. In vivo study of low back pain and shock absorption in the human locomotor system. J. Biomech. 15 (1), 21–27.

Wakeling, J.M., Liphardt, A.M., Nigg, B.M., 2003. Muscle activity reduces soft-tissue resonance at heel-strike during walking. J. Biomech. 36 (12), 1761–1769.

Wu, Z., Ovaert, T.C., Niebur, G.L., 2012. Viscoelastic properties of human cortical bone tissue depend on gender and elastic modulus. J. Orthop. Res. 30 (5), 693–699.

Yang, L., Gong, H., Zhang, M., 2012. Transmissibility of whole body vibration stimuli through human body in different standing postures. J. Mech. Med. Biol. 12 (3).

Zadpoor, A.A., Nikooyan, A.A., 2011. The relationship between lower-extremity stress fractures and the ground reaction force: a systematic review. Clin. Biomech. (Bristol, Avon) 26 (1), 23–28.